

## Pressure-densified new rhombohedral phase of $\text{EuSn}_2\text{As}_2$

Jian-Tao Wang <sup>1,2,3,\*</sup>, Changhao Wang <sup>4</sup>, and Changfeng Chen<sup>5</sup>

<sup>1</sup>Beijing National Laboratory for Condensed Matter Physics and Institute of Physics, Chinese Academy of Sciences, Beijing 100190, China

<sup>2</sup>School of Physical Sciences, University of Chinese Academy of Sciences, Beijing 100049, China

<sup>3</sup>Songshan Lake Materials Laboratory, Dongguan, Guangdong 523808, China

<sup>4</sup>Faculty of Materials and Manufacturing, Beijing University of Technology, Beijing 100124, China

<sup>5</sup>Department of Physics and Astronomy, University of Nevada, Las Vegas, Nevada 89154, USA

 (Received 22 July 2021; revised 6 October 2021; accepted 29 November 2021; published 7 December 2021)

The magnetic topological insulator  $\text{EuSn}_2\text{As}_2$  is known to crystallize in a  $\text{Bi}_2\text{Te}_3$ -type layered structure in rhombohedral symmetry at ambient conditions and undergo a structural phase transition toward a monoclinic  $\beta$  phase under increasing pressure. Here, we identify by *ab initio* calculations a new high-pressure rhombohedral structure (termed the  $\gamma$  phase) in  $R\bar{3}m$  symmetry comprising Sn-As-As-Sn linear chains along the  $z$  axis via the formation of As-As bonds in the AsSn/SnAs bilayers with strong anisotropic lattice distortion along the [001] orientation. This pressure-densified new rhombohedral phase has a metallic A-type antiferromagnetic ground state and is energetically more favorable than the original rhombohedral structure and the monoclinic  $\beta$  phase above 11 GPa. Simulated x-ray diffraction patterns provide an excellent match to the previously unexplained distinct diffraction peak around  $14.7^\circ$  found in experiments for  $\text{EuSn}_2\text{As}_2$  above 13 GPa. These findings offer key insights into a new type of high-pressure phase of layered magnetic topological insulators, laying a foundation for further exploration of this intriguing class of materials.

DOI: [10.1103/PhysRevB.104.L220101](https://doi.org/10.1103/PhysRevB.104.L220101)

Magnetic topological insulators (MTIs) have attracted tremendous research interest because they can potentially host a variety of exotic topological quantum states, such as the quantum anomalous Hall effect, Majorana bound states, and axion insulator states [1–15]. First-principles calculations have predicted a series of layered intrinsic MTIs from the tetradymite-type  $\text{MnBi}_2\text{Te}_4$ -related ternary chalcogenides [16], which have been synthesized in forms of single crystals or epitaxial films [13,17–22]. Meanwhile, a new series of layered MTIs from the Eu-based Zintl or Zintl-Klemm phases [23–28] including  $\text{EuSn}_2\text{As}_2$  [23–25] has been identified recently by first-principles calculations and experiments.

At ambient conditions,  $\text{EuSn}_2\text{As}_2$  [23] (hereafter referred to as  $\alpha$ - $\text{EuSn}_2\text{As}_2$ ) adopts a  $\text{Bi}_2\text{Te}_3$ -type structure [29–32] in rhombohedral ( $R\bar{3}m$ ) symmetry, comprising six buckled  $[\text{SnAs}]^-$  layers and three  $\text{Eu}^{2+}$  layers in an ABC stacking along the out-of-plane direction. The  $\text{Eu}^{2+}$  ions are coupled ferromagnetically within each layer and antiferromagnetically across the AsSn/SnAs bilayers, forming a three-dimensional A-type antiferromagnetic (AFM) order [23,25]. Magnetic susceptibility measurements suggested that  $\text{EuSn}_2\text{As}_2$  undergoes an AFM transition with a Néel temperature  $T_N \sim 24$  K [23–25]. Combining *ab initio* calculations and *in situ* x-ray diffraction (XRD) measurements, a monoclinic network structure of  $\beta$ - $\text{EuSn}_2\text{As}_2$  in  $C2/m$  symmetry has been found to exist under pressures above 14 GPa, and the high-pressure phase is characterized by two notable diffraction peaks around  $14^\circ$ – $15^\circ$  [33]. More recently, a distinct diffraction peak around

$14.7^\circ$  was observed above 13 GPa in *in situ* synchrotron XRD measurements [34], but the related high-pressure structural phase that produces this new XRD feature remains to be clarified.

In this Letter, we identify by *ab initio* calculations a distinct compressed phase of  $\text{EuSn}_2\text{As}_2$  that has a rhombohedral lattice in  $R\bar{3}m$  symmetry, which is shared by the experimentally identified ambient-pressure phase [23–25]. This new high-pressure rhombohedral structure (hereafter referred to as  $\gamma$ - $\text{EuSn}_2\text{As}_2$ ) is denser than the original  $\alpha$ - $\text{EuSn}_2\text{As}_2$  with about 10% volume reduction. It is energetically more stable than the layered  $\alpha$  phase and the reported monoclinic  $\beta$  phase [33] above 11 GPa. Kinetic phase conversion calculations show that this new  $\gamma$  phase can be realized via the formation of As-As bonds in the compressed AsSn/SnAs bilayers with a strong anisotropic lattice distortion along the [001] orientation; in comparison, the monoclinic  $\beta$  phase can be formed via the formation of As-As bonds across the Eu layers with a strong *shear deformation* assisted expansion along the [210] orientation. Simulated XRD patterns for the  $\gamma$  phase provide an excellent match to the previously unexplained distinct diffraction peak around  $14.7^\circ$  found in experiments for  $\text{EuSn}_2\text{As}_2$  above 13 GPa [34]. These results shed new light on the intricate structural evolution mechanisms of the layered topological materials under pressure, opening paths for further in-depth explorations of this class of novel quantum materials.

We have performed a structure search based on a layer-by-layer slip reconstruction mechanism along the [100] and [210] orientations of  $\alpha$ - $\text{EuSn}_2\text{As}_2$ , which has been employed in the structure search in graphite [35] under pressure. This targeted search resulted in the identification of  $\gamma$ - $\text{EuSn}_2\text{As}_2$  in a simple

\*wjt@aphy.iphy.ac.cn

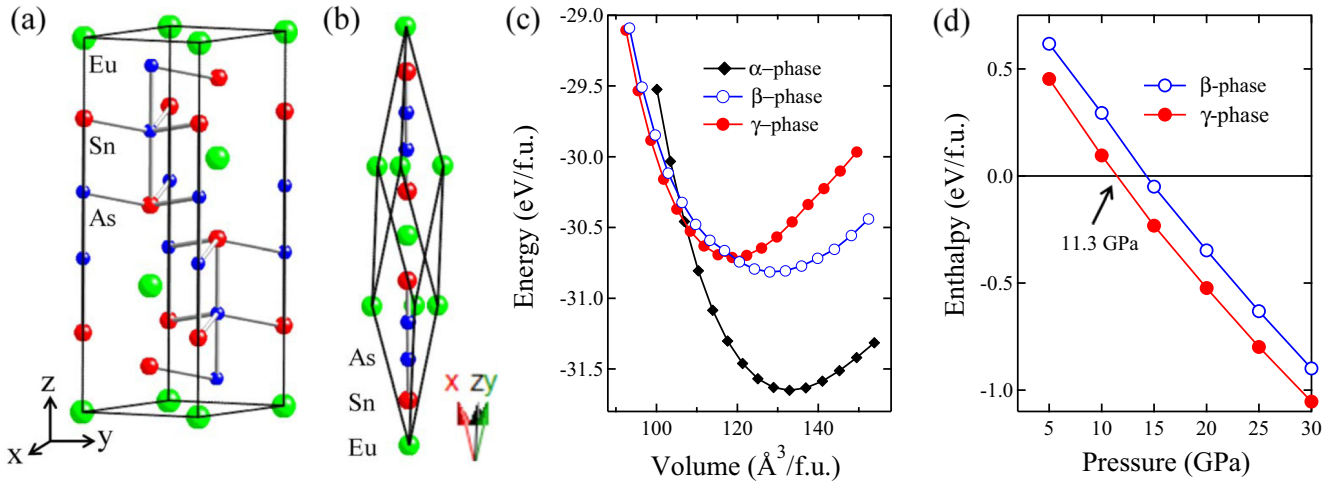


FIG. 1. (a) Crystal structure of  $\gamma$ -EuSn<sub>2</sub>As<sub>2</sub> in rhombohedral ( $R\bar{3}m$ ) symmetry at 15 GPa. The lattice parameters  $a = 4.813 \text{ \AA}$ ,  $c = 14.905 \text{ \AA}$ , and  $\gamma = 120^\circ$ . The Eu, Sn, and As atoms are occupying the  $3a$  (0.0, 0.0, 0.0),  $6c$  (0.0, 0.0, 0.2140), and  $6c$  (0.0, 0.0, 0.4139) Wyckoff positions, respectively. (b) Rhombohedral AFM primitive cell of  $\gamma$ -EuSn<sub>2</sub>As<sub>2</sub> in  $R\bar{3}m$  symmetry at 15 GPa. The lattice parameters  $a = 10.318 \text{ \AA}$  and  $\alpha = 26.98^\circ$ . The Eu, Sn, and As atoms are occupying the  $1a$  (0.0, 0.0, 0.0)-Eu (up-spin),  $1b$  (0.5, 0.5, 0.5)-Eu (down-spin),  $2c$  (0.1070, 0.1070, 0.1070)-Sn,  $2c$  (0.6070, 0.6070, 0.6070)-Sn,  $2c$  (0.2069, 0.2069, 0.2069)-As, and  $2c$  (0.7070, 0.7070, 0.7070)-As Wyckoff positions. It is corresponding to a doubled crystal cell of (a) [25]. (c) Calculated energies vs volume per formula for  $\alpha$ -,  $\beta$ -, and  $\gamma$ -EuSn<sub>2</sub>As<sub>2</sub> in A-, G-, and A-type AFM states, respectively (see Fig. S1 in the Supplemental Material [36]). (d) Enthalpy of  $\gamma$ - and  $\beta$ -EuSn<sub>2</sub>As<sub>2</sub> relative to the  $\alpha$  phase as a function of pressure.

monoclinic supercell including four Eu, eight Sn, and eight As atoms to simulate the AFM interaction of Eu atoms [33] (see details in Figs. S1 and S2 in the Supplemental Material [36]). Our density functional theory calculations are performed using the Vienna *ab initio* simulation package [37] with the all-electron projector augmented-wave method [38]. The Perdew-Burke-Ernzerhof generalized gradient approximation revised for solids (PBEsol-GGA) [39] exchange-correlation functional is adopted for the evaluation of structural and magnetic stability of EuSn<sub>2</sub>As<sub>2</sub> under pressure. The valence states  $5s^2 6s^2 5p^6 4f^7$  for Eu,  $5s^2 5p^2$  for Sn, and  $4s^2 4p^3$  for As are used with the energy cutoff of 700 eV for the plane-wave basis set. The Brillouin-zone sampling is performed using a  $9 \times 9 \times 9$   $k$ -point grid for both  $\alpha$ - and  $\gamma$ -EuSn<sub>2</sub>As<sub>2</sub>. The Hubbard  $U = 5 \text{ eV}$  [40] is used to treat the localized  $4f$  electrons of Eu in the GGA +  $U$  scheme [41]. All of the calculations including the crystal structure optimization are carried out with GGA +  $U$ . Electronic band structures and magnetic anisotropy energy are calculated with spin-orbit coupling (SOC). Phonon calculations are performed using the PHONOPY package [42].

We first characterize the crystal structure of  $\gamma$ -EuSn<sub>2</sub>As<sub>2</sub>, which has a rhombohedral lattice in  $R\bar{3}m$  (No. 166) symmetry in an ABC stacking, which is also shared by the experimentally identified ambient-pressure phase [23–25]. In the hexagonal representation [Fig. 1(a)], the calculated lattice parameters at 0 GPa are  $a = 5.066 \text{ \AA}$ ,  $c = 16.023 \text{ \AA}$ , and  $\gamma = 120^\circ$  with three inequivalent crystallographic sites, occupying the  $3a$  (0.0, 0.0, 0.0),  $6c$  (0.0, 0.0, 0.2126), and  $6c$  (0.0, 0.0, 0.4186) positions for Eu, Sn, and As atoms, respectively. The bond lengths are of 2.607  $\text{\AA}$  for As-As, 2.980–3.301  $\text{\AA}$  for As-Sn, and 3.275  $\text{\AA}$  for Sn-Sn. The calculated energetic data establish the following stability sequence:  $\gamma$  phase <  $\beta$  phase <  $\alpha$  phase at equilibrium lattice param-

eters [see Fig. 1(c)]. Upon compression, the  $\gamma$  phase becomes stable relative to the  $\alpha$  phase above 11.3 GPa [see Fig. 1(d)], and it is more stable than the  $\beta$  phase with a substantial energy gain of  $\sim 0.18 \text{ eV}$  per formula (f.u.) up to 30 GPa. The calculated lattice parameters at 15 GPa are estimated to be  $a = 4.813 \text{ \AA}$ ,  $c = 14.905 \text{ \AA}$ , and  $\gamma = 120^\circ$  with three inequivalent crystallographic sites, occupying the  $3a$  (0.0, 0.0, 0.0),  $6c$  (0.0, 0.0, 0.2140), and  $6c$  (0.0, 0.0, 0.4139) positions for Eu, Sn, and As atoms, respectively. The bond lengths are of 2.567  $\text{\AA}$  for As-As, 2.838–2.979  $\text{\AA}$  for As-Sn, and 3.117  $\text{\AA}$  for Sn-Sn. Such short bonds lead to the formation of Sn-As-As-Sn linear chains along the  $z$  axis [see Fig. 1(a)]. The calculated lattice parameters ( $a$  and  $c$ ) for both  $\alpha$ - and  $\gamma$ -EuSn<sub>2</sub>As<sub>2</sub> are listed in Table I and plotted in Fig. S3 as a function of pressure in the Supplemental Material [36]. This new  $\gamma$  phase can be considered as a denser form of  $\alpha$ -EuSn<sub>2</sub>As<sub>2</sub> with about  $-10.8\%$  to  $-8.7\%$  volume reduction from 0 to 30 GPa. We have also calculated the phonon band structures at 0 and 15 GPa using a rhombohedral AFM primitive cell [see Fig. 1(b)]. No imaginary frequency modes are observed in the entire Brillouin zone, thus confirming its dynamical stability (see Fig. S4 in the Supplemental Material [36]).

It is worth noting that the  $\alpha$  phase has a spin phase transition from A-type AFM to a ferromagnetic (FM) state around 14 GPa (see Fig. S2 in the Supplemental Material [36]), as the findings in EuCd<sub>2</sub>As<sub>2</sub> [43], while the  $\gamma$  phase has an A-type AFM ground state, which is more stable than the FM state with an energy gain of  $-5.05$  to  $-6.12 \text{ meV/f.u.}$  from 5 to 30 GPa. Because the spin phase transition pressure in the  $\alpha$  phase is larger than the crystal structure transition pressure of 11.3 GPa, the FM state is suppressed and the AFM state remains the ground state throughout the pressure range [34]. The spin moments on Eu sites derived from the  $4f$  electrons are calculated to be  $6.93\mu_B$ – $6.96\mu_B$  and prefer to lie in the

TABLE I. Calculated lattice parameters at 0, 10, 15, and 20 GPa for  $\alpha$ -EuSn<sub>2</sub>As<sub>2</sub> ( $R\bar{3}m$ ),  $\beta$ -EuSn<sub>2</sub>As<sub>2</sub> ( $C2/m$ ), and  $\gamma$ -EuSn<sub>2</sub>As<sub>2</sub> ( $R\bar{3}m$ ) phases, compared to the reported experimental data [23,33] at 0.16, 11, and 18.8 GPa.

Structure	Method	$a$ (Å)	$b$ (Å)	$c$ (Å)	$\beta$ (deg)	$P$ (GPa)
$\alpha$ -EuSn <sub>2</sub> As <sub>2</sub>	Calc.	4.202		26.157		0
	Calc.	4.055		24.246		10
	Calc.	4.019		23.502		15
	Expt. [23]	4.207		26.473		0
	Expt. [33]	4.213		26.354		0.16
	Expt. [33]	4.112		24.589		11
$\beta$ -EuSn <sub>2</sub> As <sub>2</sub>	Calc. [33]	10.584	3.596	7.659	138.95	20
	Expt. [33]	10.928	3.474	8.242	138.69	18.8
$\gamma$ -EuSn <sub>2</sub> As <sub>2</sub>	Calc.	5.066		16.023		0
	Calc.	4.881		15.155		10
	Calc.	4.813		14.905		15
	Calc.	4.755		14.704		20

$ab$  plane in the  $\gamma$  phase or parallel to the  $c$  axis in the  $\alpha$  phase (see Fig. S2). Beside the MTI behavior of the  $\alpha$  phase at ambient conditions [25], our calculated electronic band structures and density of states (DOS) show that  $\gamma$ -EuSn<sub>2</sub>As<sub>2</sub> exhibits a typical metallic character and the states around the Fermi level ( $E_F$ ) are mainly contributed by the Sn  $5p$  and As  $4p$  bands (see Fig. 2 and Fig. S5 in the Supplemental Material [36]). The Eu  $4f$  bands with SOC are very localized in an energy range of  $-1.0$  to  $-1.9$  eV below  $E_F$ , similar to that observed in EuSn<sub>2</sub>P<sub>2</sub> [28], and thus the effect of SOC on the states near  $E_F$  is very limited.

To establish the experimental connection of this new  $\gamma$  phase, we compare its simulated XRD spectra [Fig. 3(c)], along with those of the  $\alpha$  phase [Fig. 3(b)] and  $\beta$  phase [Fig. 3(d)], to the available experimental data [Fig. 3(a)] reported by Zhao *et al.* [33] (exp-1 at 0.16 GPa and exp-3 at 21.5 GPa) and Sun *et al.* [34] (exp-2 at 21.1 GPa). As shown in Fig. 3(a), there are two main peaks around  $12^\circ$  and  $17^\circ$  at 0.16 GPa (exp-1). The peak around  $12^\circ$  can be attributed to the (015) diffraction peak for  $\alpha$ -EuSn<sub>2</sub>As<sub>2</sub> [23], while the peak around  $17^\circ$  corresponds to the mix of two close peaks

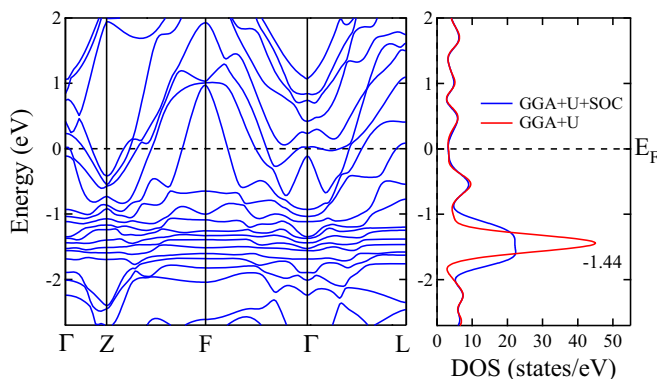


FIG. 2. Electronic band structures and total density of states (DOS) for  $\gamma$ -EuSn<sub>2</sub>As<sub>2</sub> at 15 GPa in a rhombohedral AFM primitive cell [see Fig. 1(b)] by the GGA +  $U$  + SOC method.

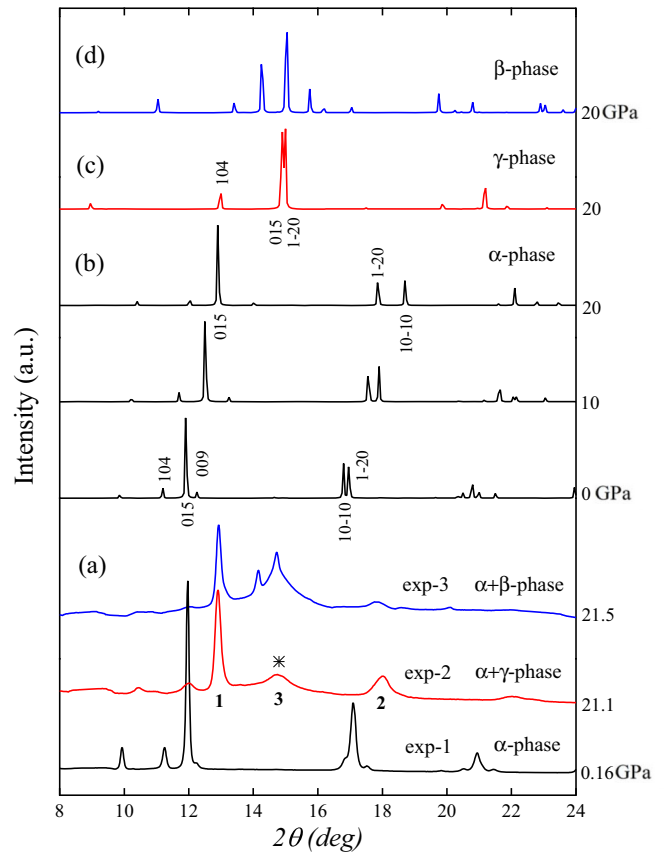


FIG. 3. (a) Experimental XRD patterns for EuSn<sub>2</sub>As<sub>2</sub> at 0.16, 21.1, and 21.5 GPa [33,34]. Two main peaks around  $12^\circ$  and  $17^\circ$  in exp-1 are shifted to  $13^\circ$  (peak 1) and  $18^\circ$  (peak 2) in exp-2 and exp-3, respectively. (b) Simulated XRD patterns for the  $\alpha$  phase at 0, 10, and 20 GPa. (c), (d) Simulated XRD patterns for the (c)  $\gamma$  phase and (d)  $\beta$  phase, at 20 GPa. The synchrotron x-ray wavelength  $\lambda = 0.6199$  Å.

( $10\bar{1}0$ ) and ( $1\bar{2}0$ ) [see Fig. 3(b) at 0 GPa]. Upon compression, the peaks around  $12^\circ$  and  $17^\circ$  in exp-1 are shifted to  $13^\circ$  (peak 1) and  $18^\circ$  (peak 2) in exp-2, respectively. Meanwhile, there is a prominent new peak around  $14.7^\circ$  (peak 3) in exp-2. Experimentally, this distinct diffraction peak appears above  $\sim 13$  GPa upon compression and can be preserved during the decompression process [34], suggesting that a new crystalline phase has been produced under high pressure. Our simulated XRD patterns show that the main diffraction peaks (015) and ( $1\bar{2}0$ ) in Fig. 3(c) for  $\gamma$ -EuSn<sub>2</sub>As<sub>2</sub> perfectly matches this broadened peak 3. In other words, the new diffraction peak around  $14.7^\circ$  in exp-2 can be attributed to the mixture of two closely positioned peaks (015) and ( $1\bar{2}0$ ) of  $\gamma$ -EuSn<sub>2</sub>As<sub>2</sub> (more details are given in Fig. S6 in the Supplemental Material [36]). In addition, in exp-3 [33], there are two distinct diffraction peaks around  $14^\circ$ – $15^\circ$ , which are clearly different from the new peak 3 in exp-2, but match better with the simulated XRD patterns [see Fig. 3(d)] for the monoclinic  $\beta$  phase [33]. These XRD data suggest that the densified new rhombohedral  $\gamma$  phase as well as the reported monoclinic  $\beta$  phase [33] is a high-pressure phase for EuSn<sub>2</sub>As<sub>2</sub>.

Based on our proposed  $\gamma$ -EuSn<sub>2</sub>As<sub>2</sub> structure and the simulated XRD patterns [see Fig. 3(c) at 20 GPa], we have further

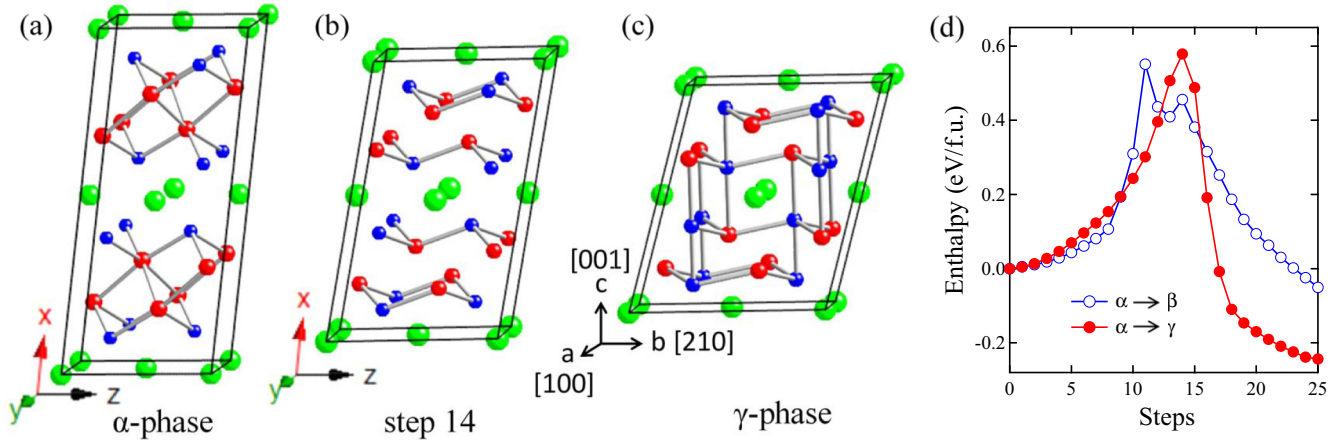


FIG. 4. Phase conversion from the  $\alpha$  phase toward the  $\gamma$  phase for  $\text{EuSn}_2\text{As}_2$  at 15 GPa in  $R\bar{3}m$  symmetry. (a) The initial geometry of the  $\alpha$  phase in a monoclinic supercell with the connecting of Sn-Sn atoms between the buckled SnAs layers. (b) The key structure at step 14 between the  $\alpha$  and  $\gamma$  phase with breaking of Sn-Sn bonds. (c) Structure at step 25 for  $\gamma$ - $\text{EuSn}_2\text{As}_2$  with the formation of As-As bonds in the AsSn/SnAs bilayer. The lattice orientations corresponding to the hexagonal lattice are indicated in (c). (d) Enthalpy vs pathway at 15 GPa for the transformations from the  $\alpha$  phase toward the  $\beta$  and  $\gamma$  phases.

refined the powder XRD pattern in exp-2 [34] by the Rietveld method [44] through the FULLPROF software [45]. As shown in Fig. S7 in the Supplemental Material [36], the calculated XRD patterns are in good agreement with the experimental XRD patterns. The refinement  $R$  factors for exp-2 at 21.1 GPa are  $R_p = 1.53\%$  and  $R_{wp} = 2.11\%$ . We can see that the XRD patterns in exp-2 [34] are indeed a mixed phase composed of both  $\alpha$  and  $\gamma$  structures.

We finally explore the underlying dynamic process for the phase transformation from  $\alpha$ - $\text{EuSn}_2\text{As}_2$  toward the denser  $\gamma$ - $\text{EuSn}_2\text{As}_2$  phase, using the modified climbing image nudged elastic band method [46,47]. The key structural snapshots and the enthalpy changes along the pathways are plotted in Fig. 4. Throughout the pathway from  $\alpha$ - toward  $\gamma$ - $\text{EuSn}_2\text{As}_2$ , as shown in Figs. 4(a)–4(c), the lattice parameters  $a[100]$  and  $b[210]$  are about 18.8% expanded, while  $c$  is about  $-35.8\%$  compressed, respectively, showing a strong anisotropic lattice distortion along the  $c[001]$  orientation. The energy increases initially due to the increasing of in-plane strain in the AsSn/SnAs bilayer and achieves an energy peak (0.58 eV/f.u.) around step 14 [Fig. 4(d)] with the bond breaking between Sn-Sn atoms [see Fig. 4(b)]; upon overcoming this peak, the energy decreases due to the formation of As-As bonds in the compressed AsSn/SnAs bilayer and finally form the new  $\gamma$  phase [Fig. 4(c)] with the formation of Sn-As-As-Sn chains along the  $[001]$  orientation.

Meanwhile, for comparison, we have also explored the underlying dynamic conversion process from the  $\alpha$  phase toward the  $\beta$  phase. Throughout the pathway (see details in Fig. S8 in the Supplemental Material [36]), the lattice parameters  $a[100]$  and  $c[001]$  are about  $-11.4\%$  and  $-35.4\%$  compressed, while  $b[210]$  is about 48.3% expanded, respectively, showing a strong pressure-induced *shear deformation*, similar to the findings in graphite [48]. With the increase of shear deformation, the energy increases initially due to the some bond breaking of As-Sn bonds in the AsSn/SnAs

bilayer, and achieves an energy peak (0.55 eV/f.u.) [see Fig. 4(d)] around step 11; and then the energy decreases with the formation of As-As bonds across the Eu layers to form the  $\beta$  phase via the *shear deformation* process along the  $[210]$  orientation. These results suggest two competing conversion pathways toward the  $\gamma$  or  $\beta$  phase via the formation of As-As bonds in the AsSn/SnAs bilayers or across the Eu layers, respectively.

In summary, we have identified a new high-pressure  $\gamma$  phase for  $\text{EuSn}_2\text{As}_2$  in  $R\bar{3}m$  symmetry by *ab initio* calculations. This pressure-densified new rhombohedral  $\gamma$  phase of  $\text{EuSn}_2\text{As}_2$  can be realized by a strong anisotropic lattice distortion along the  $[001]$  orientation accompanied by the formation of As-As bonds in AsSn/SnAs bilayers, in contrast to the distinct mechanism of the *shear deformation* process in forming the  $\beta$  phase along the  $[210]$  orientation via the formation of As-As bonds across the Eu layers. Total energy calculations show that the  $\gamma$  phase is more stable than the  $\alpha$  phase and previously reported monoclinic  $\beta$  phase above  $\sim 11$  GPa. Simulated XRD patterns provide an excellent match to the previously unexplained distinct diffraction peak around  $14.7^\circ$  found in experiments for  $\text{EuSn}_2\text{As}_2$  above 13 GPa [34]. Moreover, we find that  $\gamma$ - $\text{EuSn}_2\text{As}_2$  has a metallic A-type antiferromagnetic ground state. These discoveries provide a comprehensive energetics and kinetics understanding of the intricate pressure-induced structural transformation routes and the underpinning mechanisms. The present results provide an excellent account for the pressure evolution of the layered magnetic topological materials, laying a foundation for further studies of these fascinating materials.

We are grateful to Hongming Weng for valuable discussions. This work was supported by the National Key Research and Development Program of China (Grant No. 2020YFA0711502), the National Natural Science Foundation of China (Grants No. 11974387 and No. 11804012), and the

Strategic Priority Research Program of the Chinese Academy of Sciences (Grant No. XDB33000000). C.W. acknowledges

support from the Beijing Municipal Education Commission (Grant No. KM201910005009).

- [1] Q. Liu, C. X. Liu, C. Xu, X. L. Qi, and S. C. Zhang, *Phys. Rev. Lett.* **102**, 156603 (2009).
- [2] R. S. K. Mong, A. M. Essin, and J. E. Moore, *Phys. Rev. B* **81**, 245209 (2010).
- [3] N. Kurita, M. Kimata, K. Kodama, A. Harada, M. Tomita, H. S. Suzuki, T. Matsumoto, K. Murata, S. Uji, and T. Terashima, *Phys. Rev. B* **83**, 214513 (2011).
- [4] K. Matsubayashi, K. Munakata, M. Isobe, N. Katayama, K. Ohgushi, Y. Ueda, Y. Uwatoko, N. Kawamura, M. Mizumaki, N. Ishimatsu, M. Hedo, and I. Umehara, *Phys. Rev. B* **84**, 024502 (2011).
- [5] C. Z. Chang, J. S. Zhang, X. Feng, J. Shen, Z. C. Zhang, M. H. Guo, K. Li, Y. B. Ou, P. Wei, L. L. Wang, Z. Q. Ji, Y. Feng, S. H. Ji, X. Chen, J. F. Jia, X. Dai, Z. Fang, S. C. Zhang, K. He, Y. Y. Wang *et al.*, *Science* **340**, 167 (2013).
- [6] M. Mogi, M. Kawamura, R. Yoshimi, A. Tsukazaki, Y. Kozuka, N. Shirakawa, K. S. Takahashi, M. Kawasaki, and Y. Tokura, *Nat. Mater.* **16**, 516 (2017).
- [7] Q. L. He, X. Kou, A. J. Grutter, G. Yin, L. Pan, X. Che, Y. Liu, T. Nie, B. Zhang, S. M. Disseler, B. J. Kirby, W. Ratcliff II, Q. Shao, K. Murata, X. Zhu, G. Yu, Y. Fan, M. Montazeri, X. Han, J. A. Borchers *et al.*, *Nat. Mater.* **16**, 94 (2017).
- [8] J. Wu, F. Liu, M. Sasase, K. Ienaga, Y. Obata, R. Yukawa, K. Horiba, H. Kumigashira, S. Okuma, T. Inoshita, and H. Hosono, *Sci. Adv.* **5**, eaax9989 (2019).
- [9] Y. Tokura, K. Yasuda, and A. Tsukazaki, *Nat. Rev. Phys.* **1**, 126 (2019).
- [10] D. Q. Zhang, M. J. Shi, T. S. Zhu, D. Y. Xing, H. J. Zhang, and J. Wang, *Phys. Rev. Lett.* **122**, 206401 (2019).
- [11] Y. Gong, J. W. Guo, J. H. Li, K. J. Zhu, M. H. Liao, X. Z. Liu, Q. H. Zhang, L. Gu, L. Tang, X. Feng, D. Zhang, W. Li, C. L. Song, L. L. Wang, P. Yu, X. Chen, Y. Y. Wang, H. Yao, W. H. Duan, Y. Xu *et al.*, *Chin. Phys. Lett.* **36**, 089901 (2019).
- [12] J. Li, C. Wang, Z. Zhang, B. L. Gu, W. H. Duan, and Y. Xu, *Phys. Rev. B* **100**, 121103(R) (2019).
- [13] M. M. Otrokov, I. P. Rusinov, M. Blanco-Rey, M. Hoffmann, A. Y. Vyazovskaya, S. V. Eremeev, A. Ernst, P. M. Echenique, A. Arnau, and E. V. Chulkov, *Phys. Rev. Lett.* **122**, 107202 (2019).
- [14] Y. J. Deng, Y. J. Yu, M. Z. Shi, Z. X. Guo, Z. H. Xu, J. Wang, X. H. Chen, and Y. B. Zhang, *Science* **367**, 6480 (2020).
- [15] L. Chen, D. C. Wang, C. M. Shi, C. Jiang, H. M. Liu, G. L. Cui, X. M. Zhang, and X. L. Li, *J. Mater. Sci.* **55**, 14292 (2020).
- [16] J. Li, Y. Li, S. Du, Z. Wang, B. L. Gu, S. C. Zhang, K. He, W. H. Duan, and Y. Xu, *Sci. Adv.* **5**, eaaw5685 (2019).
- [17] Y. Gong, J. W. Guo, J. H. Li, K. J. Zhu, M. H. Liao, X. Z. Liu, J. H. Zhang, L. Gu, L. Tang, X. Feng, D. Zhang, W. Li, C. L. Song, L. L. Wang, P. Yu, X. Chen, Y. X. Wang, H. Yao, W. H. Duan, Y. Xu, Q. K. Xue *et al.*, *Chin. Phys. Lett.* **36**, 076801 (2019).
- [18] C. Liu, Y. Wang, H. Li, Y. Wu, Y. Li, J. Li, K. He, Y. Xu, J. Zhang, and Y. Wang, *Nat. Mater.* **19**, 522 (2020).
- [19] G. Shi, M. Zhang, D. Yan, H. Feng, M. Yang, Y. Shi, and Y. Li, *Chin. Phys. Lett.* **37**, 047301 (2020).
- [20] H. Li, S. Liu, C. Liu, J. Zhang, Y. Xu, R. Yu, Y. Wu, Y. Zhang, and S. Fan, *Phys. Chem. Chem. Phys.* **22**, 556 (2020).
- [21] D. S. Lee, T. H. Kim, C. H. Park, C. Y. Chung, Y. S. Lim, W. S. Seo, and H. H. Park, *CrystEngComm* **15**, 5532 (2013).
- [22] J. Q. Yan, Q. Zhang, T. Heitmann, Z. Huang, K. Y. Chen, J. G. Cheng, W. Wu, D. Vaknin, B. C. Sales, and R. J. McQueeney, *Phys. Rev. Materials* **3**, 064202 (2019).
- [23] M. Q. Arguilla, N. D. Cultrara, Z. J. Baum, S. Jiang, R. D. Ross, and J. E. Goldberger, *Inorg. Chem. Front.* **4**, 378 (2017).
- [24] H. C. Chen, Z. F. Lou, Y. X. Zhou, Q. Chen, B. J. Xu, S. J. Chen, J. H. Du, J. H. Yang, H. D. Wang, and M. H. Fang, *Chin. Phys. Lett.* **37**, 047201 (2020).
- [25] H. Li, S. Y. Gao, S. F. Duan, Y. F. Xu, K. J. Zhu, S. J. Tian, J. C. Gao, W. H. Fan, Z. C. Rao, J. R. Huang, J. J. Li, D. Y. Yan, Z. T. Liu, W. L. Liu, Y. B. Huang, Y. L. Li, Y. Liu, G. B. Zhang, P. Zhang, T. Kondo *et al.*, *Phys. Rev. X* **9**, 041039 (2019).
- [26] Y. F. Xu, Z. D. Song, Z. J. Wang, H. Weng, and X. Dai, *Phys. Rev. Lett.* **122**, 256402 (2019).
- [27] F. H. Yu, H. M. Mu, W. Z. Zhuo, Z. Y. Wang, Z. F. Wang, J. J. Ying, and X. H. Chen, *Phys. Rev. B* **102**, 180404(R) (2020).
- [28] X. Gui, I. Pletikoscic, H. B. Cao, H. J. Tien, X. T. Xu, R. D. Zhong, G. Q. Wang, T. R. Chang, S. Jia, T. Valla, W. W. Xie, and R. J. Cava, *ACS Cent. Sci.* **5**, 900 (2019).
- [29] H. J. Zhang, C. X. Liu, X. L. Qi, X. Dai, Z. Fang, and S. C. Zhang, *Nat. Phys.* **5**, 438 (2009).
- [30] R. Vilaplana, D. Santamaria-Perez, O. Gomis, F. J. Manjon, J. Gonzalez, A. Segura, A. Munoz, P. Rodriguez-Hernandez, E. Perez-Gonzalez, V. Marin-Borras, V. Munoz-Sanjose, C. Drasar, and V. Kucek, *Phys. Rev. B* **84**, 184110 (2011).
- [31] S. J. Zhang, J. L. Zhang, X. H. Yu, J. Zhu, P. P. Kong, S. M. Feng, Q. Q. Liu, L. X. Yang, X. C. Wang, L. Z. Cao, W. G. Yang, L. Wang, H. K. Mao, Y. S. Zhao, H. Z. Liu, X. Dai, Z. Fang, S. C. Zhang, and C. Q. Jin, *J. Appl. Phys.* **111**, 112630 (2012).
- [32] L. Zhu, H. Wang, Y. C. Wang, J. A. Lv, Y. M. Ma, Q. L. Cui, Y. M. Ma, and G. T. Zou, *Phys. Rev. Lett.* **106**, 145501 (2011).
- [33] L. Zhao, C. J. Yi, C. T. Wang, Z. H. Chi, Y. Y. Yin, X. L. Ma, J. H. Dai, P. T. Yang, B. B. Yue, J. G. Cheng, Fang Hong, J. T. Wang, Y. H. Han, Y. G. Shi, and X. H. Yu, *Phys. Rev. Lett.* **126**, 155701 (2021).
- [34] H. Sun, C. Chen, Y. Hou, W. Wang, Y. Gong, M. Huo, L. Li, J. Yu, W. Cai, N. Liu, R. Wu, D.-X. Yao, and M. Wang, *Sci. China-Phys. Mech. Astron.* **64**, 118211 (2021).
- [35] J. T. Wang, C. F. Chen, and Y. Kawazoe, *Phys. Rev. Lett.* **106**, 075501 (2011).
- [36] See Supplemental Material at <http://link.aps.org/supplemental/10.1103/PhysRevB.104.L220101> for the structure search procedure (Sec. 1); the magnetic spin configurations (Fig. S1) and relative stability (Fig. S2); the calculated lattice parameters for  $\alpha$ - and  $\gamma$ -EuSn<sub>2</sub>As<sub>2</sub> (Fig. S3); the phonon band structures for  $\gamma$ -EuSn<sub>2</sub>As<sub>2</sub> (Fig. S4); the calculated electronic band structures without SOC for  $\gamma$ -EuSn<sub>2</sub>As<sub>2</sub> (Fig. S5); the simulated (015)

- and  $(1\bar{2}0)$  peak positions for  $\alpha$ - and  $\gamma$ -EuSn<sub>2</sub>As<sub>2</sub> (Fig. S6); the refined XRD patterns for exp-2 at 21.1 GPa (Fig. S7); and the pathway from the  $\alpha$  phase toward the  $\beta$  phase at 15 GPa (Fig. S8), which includes Refs. [25,33–35,43–48].
- [37] G. Kresse and J. Furthmüller, *Phys. Rev. B* **54**, 11169 (1996).
- [38] P. E. Blöchl, *Phys. Rev. B* **50**, 17953 (1994).
- [39] J. P. Perdew, A. Ruzsinszky, G. I. Csonka, O. A. Vydrov, G. E. Scuseria, L. A. Constantin, X. Zhou, and K. Burke, *Phys. Rev. Lett.* **100**, 136406 (2008).
- [40] With the pressure change from 5 to 30 GPa, the change of “the energy position of Eu 4*f* bands” for  $\gamma$ -EuSn<sub>2</sub>As<sub>2</sub> in Fig. 2 is estimated to be from  $-1.40$  to  $-1.51$  eV and the  $U$  value should change to 4.9 or 5.1 eV.
- [41] V. I. Anisimov, J. Zaanen, and O. K. Andersen, *Phys. Rev. B* **44**, 943 (1991).
- [42] A. Togo, F. Oba, and I. Tanaka, *Phys. Rev. B* **78**, 134106 (2008).
- [43] E. Gati, S. L. Bud’ko, L. L. Wang, A. Valadkhani, R. Gupta, B. Kuthanazhi, L. Xiang, J. M. Wilde, A. Sapkota, Z. Guguchia, R. Khasanov, R. Valenti, and P. C. Canfield, *Phys. Rev. B* **104**, 155124 (2021).
- [44] H. M. Rietveld, *J. Appl. Crystallogr.* **2**, 65 (1969).
- [45] J. Rodriguez-Carvajal, *Phys. B: Condens. Matter* **192**, 55 (1993).
- [46] J. T. Wang, C. F. Chen, H. Mizuseki, and Y. Kawazoe, *Phys. Rev. Lett.* **110**, 165503 (2013).
- [47] G. Henkelman, B. P. Uberuaga, and H. Jónsson, *J. Chem. Phys.* **113**, 9901 (2000).
- [48] J. Dong, Z. Yao, M. Yao, R. Li, K. Hu, L. Zhu, Y. Wang, H. Sun, B. Sundqvist, K. Yang, and B. B. Liu, *Phys. Rev. Lett.* **124**, 065701 (2020).